

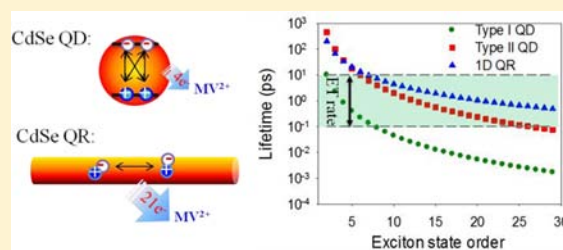
# Enhanced Multiple Exciton Dissociation from CdSe Quantum Rods: The Effect of Nanocrystal Shape

Haiming Zhu and Tianquan Lian\*

Department of Chemistry, Emory University, Atlanta, Georgia 30322, United States

**S** Supporting Information

**ABSTRACT:** A unique ability of semiconductor nanocrystals (NCs) is the generation and accommodation of multiple excitons through either optical or electric current pumping. The development and improvement of NC-based optoelectronic devices that utilize multiple excitons requires the understanding of multiple exciton dynamics and their efficient conversion to emitted photons or external charges prior to exciton–exciton annihilation. Here, we demonstrate that significantly enhanced multiexciton dissociation efficiency can be achieved in CdSe quantum rods (QRs) compared to CdSe quantum dots (QDs). Using transient absorption spectroscopy, we reveal the formation of bound one-dimensional exciton states in CdSe QRs and that multiple exciton Auger recombination occurs primarily via exciton–exciton collision. Furthermore, quantum confinement in the QR radial direction facilitates ultrafast exciton dissociation by interfacial electron transfer to adsorbed acceptors. Under high excitation intensity, more than 21 electrons can be transferred from one CdSe QR to adsorbed methylviologen molecules, greatly exceeding the multiexciton dissociation efficiency of CdSe QDs.



## INTRODUCTION

Quantum confined colloidal semiconductor nanocrystals (NCs) have been a subject of intense interests because of their size-dependent optical and electronic properties, processing versatility and low cost. In addition, these NCs can generate and accommodate multiple excitons [electron–hole (e–h) pairs] through either optical or electric current pumping. Therefore, NCs can potentially be used in advanced optoelectronic devices ranging from high-power light-emitting diodes,<sup>1,2</sup> low-threshold lasing media,<sup>3,4</sup> and multiphoton source<sup>5,6</sup> to highly sensitive and efficient photodetectors and photovoltaic/catalytic cells.<sup>7–9</sup> The development and improvement of these NC-based devices requires the understanding of multiple exciton dynamics in NCs and their efficient conversion to emitted photons (for emission applications) or separated external charges (for photovoltaic/catalytic applications) before exciton–exciton annihilation.<sup>10–12</sup>

Multiexcitons can annihilate through Auger recombination, wherein an e–h pair nonradiatively recombines by transferring its energy to another carrier or exciton. This process occurs on the 10–100 ps time scale for biexciton states in typical CdSe QDs. The Auger recombination in QDs involves three particle collisions, and the lifetime ( $\tau_n$ ) for  $n$ -exciton state decreases rapidly with  $n$ :  $1/\tau_n = C_3/2(n^2(n-1))$ , where  $C_3$ , the three molecular Auger recombination rate constant, is related to the biexciton state recombination rate ( $C_3 = 1/2\tau_2$ ).<sup>13–16</sup> Previous proof-of-principle experiments have demonstrated that up to three<sup>17</sup> and four<sup>18</sup> excitons per CdSe QDs (generated by the absorption of multiple photons) can be dissociated by interfacial charge separation to adsorbed electron acceptors.

The number of dissociated excitons is limited by the competition between interfacial electron-transfer (ET) and exciton–exciton annihilation. To achieve high multiexciton dissociation (MED) efficiency, it is highly desirable to facilitate the interfacial charge separation while slowing down the Auger annihilation process in NCs. We previously investigated an approach for improving MED efficiency by utilizing quasi-type II CdSe/CdS core/shell QDs.<sup>19</sup> The reduced e–h overlap in the quasi-type II structure decreases the Auger recombination rate constant  $C_A$ , lengthening the lifetime of the multiple-exciton states. Furthermore, the carrier distribution also enables ultrafast electron transfer to the acceptor. As a result, up to 19 excitons can be dissociated from these QDs with methylviologen (MV<sup>2+</sup>) as the electron acceptor.<sup>19</sup>

In this paper, we report a new approach for enhancing MED efficiency by using one-dimensional (1D) quantum rods (QRs). The synthesis and photovoltaic/photocatalytic application of QRs and associated heterostructures have attracted intense interest in recent years.<sup>20–25</sup> Unlike QDs, in quantum confined nanorods (NRs) and nanowires (NWs), the e–h Coulomb interaction is dramatically enhanced by the dielectric contrast effect, leading to the formation of strongly bound 1D excitons.<sup>26–30</sup> One consequence of the 1D exciton structure is the highly polarized emission along the direction of the rod, which has been observed in the pioneering studies of QRs.<sup>20,31–34</sup> As another consequence, the Auger recombination is expected to occur through bimolecular exciton–exciton

Received: May 15, 2012

Published: June 17, 2012

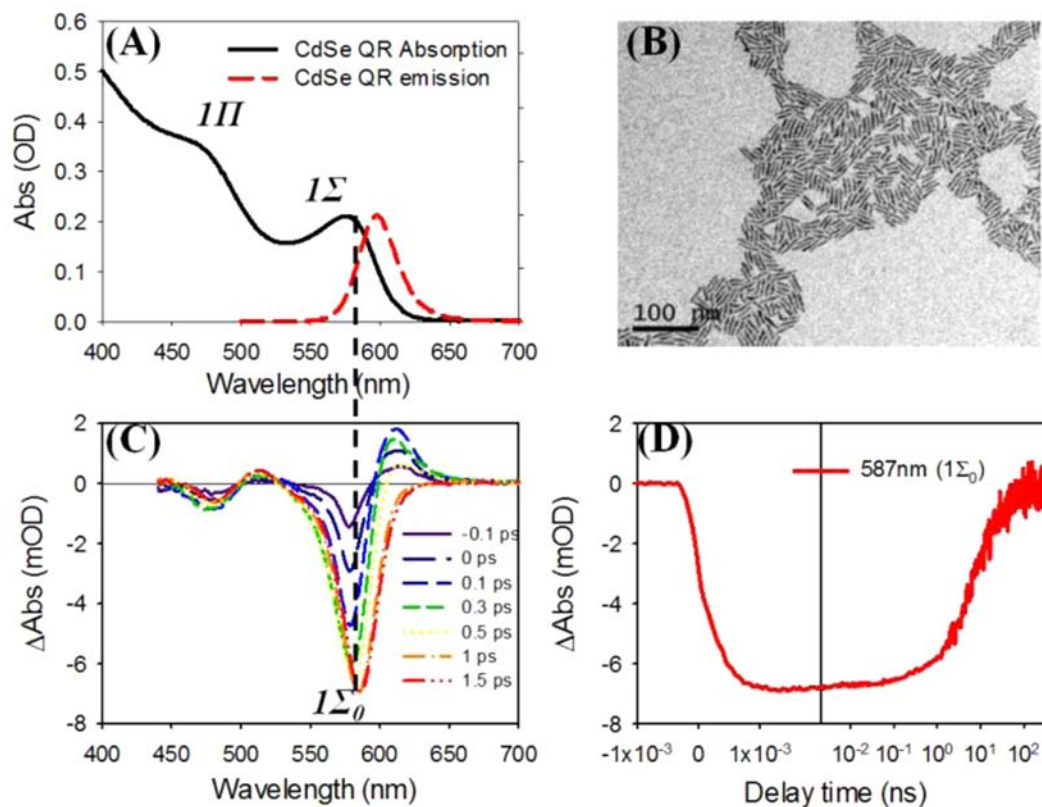


**Figure 1.** (A) Absorption and emission spectra and (B) TEM image of CdSe QRs. (C) TA spectra of CdSe QR at indicated delay times (−0.1 to 1.5 ps) after 400 nm excitation (at lowest intensity,  $7 \mu\text{J}\cdot\text{cm}^{-2}$ ). (D)  $1\Sigma_0$  (587 nm) bleach formation and decay kinetics. The left panel (−1 to 2 ps) is in linear scale, and the right panel (2 ps to 1000 ns) is in logarithmic scale.

collision, which has been suggested and probed in both CdSe QRs and NWs.<sup>15,35–37</sup> In principle, the lifetime ( $\tau_n$ ) for  $n$ -exciton state in a bimolecular recombination process can be generalized as  $1/\tau_n = C_2/2(n(n-1))$ , where bimolecular Auger recombination rate constant  $C_2 = 1/\tau_2$ .<sup>15,38</sup> Unfortunately, the experimental support for this scaling law remains incomplete because of the difficulties in extracting the lifetimes of higher order ( $n \geq 3$ ) exciton states in these previous studies.<sup>14,35</sup> The expected slower increase of exciton annihilation rate with exciton number suggests the possibility of enhanced MED efficiency in QRs. Motivated by this expectation and by reported ultrafast charge separation in CdSe QR electron-acceptor complexes,<sup>39</sup> we investigate the 1D exciton annihilation and dissociation dynamics in CdSe QRs by transient absorption (TA) spectroscopy. We first examine the 1D excitonic states and assign the spectral signatures of electrons and holes. We show that the multiexciton Auger recombination process in CdSe QR is governed by exciton–exciton bimolecular annihilation dynamics with  $1/\tau_n = C_2/2(n(n-1))$ , and the multiexciton lifetime is significantly lengthened compared with CdSe QDs. With  $\text{MV}^{2+}$  as a model electron acceptor, we demonstrate ultrafast exciton dissociation by interfacial ET ( $\sim 59$  fs) from the CdSe QR to the adsorbed  $\text{MV}^{2+}$  due to quantum confinement in the radial direction. The ultrafast charge separation and lengthened multiexciton lifetimes enable the dissociation of over 21 excitons from one CdSe QR at high excitation intensity, greatly exceeding the MED efficiency of CdSe QDs.<sup>18</sup>

## RESULTS AND DISCUSSION

### Spectral Signature and Assignment of 1D Excitons.

Phosphonic acid-capped CdSe QRs were synthesized following a published procedure with slight modification (see S11, Supporting Information for details).<sup>40</sup> From the TEM image (Figure 1B), the CdSe QR is determined to be  $3.2 \pm 0.2$  nm in diameter and  $28.9 \pm 3.1$  nm in length (aspect ratio  $\sim 9$ ). The absorption spectrum of the QR shows distinct exciton bands at 575 and 457 nm, and the exciton emission peak is centered at 600 nm with 7% quantum yield. Considering the bulk exciton Bohr radius of CdSe ( $\sim 5.6$  nm), the motion of electrons and holes is quantum confined only in the radial direction, leading to discrete electron and hole levels,  $1\sigma$ ,  $1\pi$ , etc.<sup>26,27,30</sup> Because of dielectric contrast between the rod and the surrounding medium, the e–h binding energy is significantly enhanced, giving rise to an effective Coulomb potential that depends on their separation along the long axis of the QR. This 1D potential between the  $1\sigma$  ( $\pi$ ) electron and hole forms bound  $1\Sigma$  ( $\Pi$ ) exciton states.<sup>26,27,30</sup> The density of the 1D exciton states in those bands increases quickly with energy, but the oscillator strength is largely concentrated on the lowest energy exciton state ( $1\Sigma_0$ ).<sup>26,27</sup> Following these theoretical models,<sup>26,27,30</sup> the exciton bands at 575 and 457 nm in the steady-state absorption spectrum are assigned to  $1\Sigma$  and  $1\Pi$  exciton manifolds, respectively.

The TA spectra of CdSe QRs at the lowest excitation intensity ( $7 \mu\text{J}\cdot\text{cm}^{-2}$  at 400 nm) are shown in Figure 1C (−0.1 to 1.5 ps) and in S12, Supporting Information (0–1.2 ns). Under this excitation intensity, the average number of excitons per QR is  $\sim 0.08$  (see analysis below). Upon 400 nm excitation,

higher energy exciton states are populated, which is followed by rapid intraband relaxation to the lowest energy levels indicated by the formation and decay of a positive biexciton peak at  $\sim 610$  nm and the progressive red shift and growth of the  $1\Sigma$  bleach peak (Figure 1C).<sup>41–43</sup> At  $\sim 1$  ps, the bleach signal is dominated by the state filling of the lowest energy ( $1\Sigma_0$ ) exciton state at 587 nm.<sup>41</sup> A single exponential fit to the kinetics at 587 nm yields a rise time of 0.5 ps, which represents the hot carrier relaxation time (Figure 1D). The subsequent bleach recovery, reflecting the decay of the  $1\Sigma_0$  exciton population, has a half-life time of about 4.9 ns (see Figure 1D). This 1D exciton lifetime in CdSe QRs is  $\sim 3$  times shorter than that of the 0D excitons in CdSe QDs of similar exciton energy ( $\sim 15$  ns), which is consistent with the predicted accelerated e–h recombination in QRs.<sup>26,27</sup> At 1.2 ns,  $1\Sigma_0$  bleach decays by 17% (thus the percentage of the remaining signal  $\gamma = 0.83$ ) due to single exciton recombination. The absence of any fast decay component on this time scale confirms negligible multiexciton population under such excitation conditions.

The TA spectra of CdSe QRs at 1.5 ps under different excitation intensities ( $7$ – $2390 \mu\text{J}\cdot\text{cm}^{-2}$ ) are compared in Figure 2A. The complete sets of TA spectra as a function of time ( $0$ – $1.2$  ns) are shown in SI2, Supporting Information. At 1.5 ps, when hot carrier relaxation is completed and exciton–exciton annihilation is negligible, the  $1\Sigma$  bleach in the TA spectra reflects the occupancy of exciton states. In addition to the  $1\Sigma$  bleach, the TA spectra of excited CdSe QRs also show broad and weak photoinduced absorption (PA) features at  $>650$  nm (Figure 2A inset). The PA signal shows identical kinetics in the  $650$ – $770$  nm spectral region after  $\sim 1$  ps. Before 1 ps, the kinetic traces at different wavelengths contain varying amplitudes of the biexciton peak shift signal shown in Figure 2A. In order to identify the contributions of electrons and holes to the  $1\Sigma_0$  and PA spectral signatures, selective charge-transfer studies are performed on CdSe QRs. The TA kinetics of  $1\Sigma_0$  and PA features with different acceptors can be seen in SI5, Supporting Information. Without electron or hole acceptors, the  $1\Sigma_0$  and PA signals have identical and long-lived kinetics within 1.2 ns. In the presence of benzoquinone (BQ), an electron acceptor,<sup>44,45</sup> the  $1\Sigma_0$  bleach shows an ultrafast and nearly complete decay, while the PA signal remains unaffected, indicating that the  $1\Sigma_0$  bleach is solely due to the state filling of the  $1\sigma$  electron level, while the PA feature can be attributed to the transition of holes. The selective removal of the hole by phenothiazine (PTZ), a hole acceptor,<sup>46,47</sup> leads to slightly longer-lived  $1\Sigma_0$  bleach signal and shorter-lived PA signal, further confirming the spectral assignment of these species (see SI5, Supporting Information).

In free QRs, the PA signal forms with a rise time of  $\sim 0.06$  ps (result not shown) and decays with the same kinetics as the  $1\Sigma_0$  bleach. The latter indicates that the CB electron decays mainly by recombination with the hole that is responsible for the PA signal. The lack of clear rise process suggests that the PA signal can be attributed to the photoexcited valence band (VB) hole (with negligible trapping in  $<1.2$  ns), trapped hole (with  $<0.06$  ps trapping time), or both the trapped and VB holes (with indistinguishable PA spectral feature). Although there has been reports of the hole trapping process in CdSe QDs or QRs on the  $10$ – $100$  ps time scale, it is unclear whether similar trapping time can be expected in our QRs.<sup>48,49</sup> The small fluorescence quantum yields of the QRs suggest that the holes are likely trapped and the PA signal is dominated by the trapped holes. Despite the uncertainty in the nature of the hole (VB vs

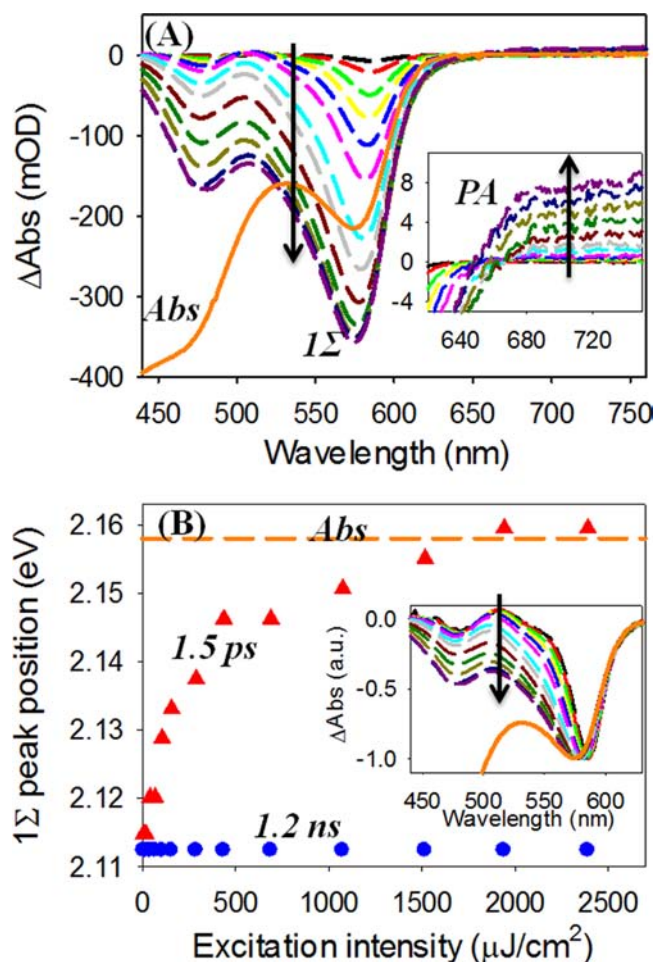


**Figure 2.** (A) TA spectra of CdSe QRs at 1.5 ps under different excitation intensities (from 7 to  $2390 \mu\text{J}\cdot\text{cm}^{-2}$ ), and the steady-state absorption spectrum of CdSe QRs (orange circles, inverted). (Inset) Expanded view of the spectra from 600 to 770 nm, showing the PA feature. (B) The  $1\Sigma$  bleach peak position at 1.5 ps (red triangles) and 1.2 ns (blue circles) as a function of the excitation intensity. The peak position of the steady-state absorption spectrum is indicated by the solid orange line. (Inset) Normalized comparison of the transient and steady-state absorption spectra shown in (A).

trapped) and the transitions involved in the PA signal, we will show below that its amplitude scales linearly with the number of excitons and can be used to follow the exciton dynamics.<sup>16,19</sup>

**Multiexciton Dynamics in CdSe QRs.** As shown in Figure 2A, the  $1\Sigma$  bleach amplitude increases at higher excitation intensity, indicating the creation of more excitons in the CdSe QR. Associated with the amplitude increase, the peak of the  $1\Sigma$  bleach shifts to higher energy, which can be better seen in the comparison of normalized TA spectra (Figure 2B inset) and the comparison of  $1\Sigma$  bleach peak positions at 1.5 ps and 1.2 ns (Figure 2B). At the lowest excitation intensity, when single exciton states dominate, the bleach peak position remains unchanged at 1.5 ps and 1.2 ns, agreeing well with the  $1\Sigma_0$  peak position and red shifted from the steady-state  $1\Sigma$  peak. With increasing excitation intensity, when more excitons are created in each QR, the  $1\Sigma$  bleach at 1.5 ps shows increased amplitude on the higher energy side, broadened line width, and blue-shifted peak position. At the highest excitation intensity ( $2390 \mu\text{J}\cdot\text{cm}^{-2}$ ), the transient spectra gradually approach the steady-state absorption spectrum of the  $1\Sigma$  band. The observed

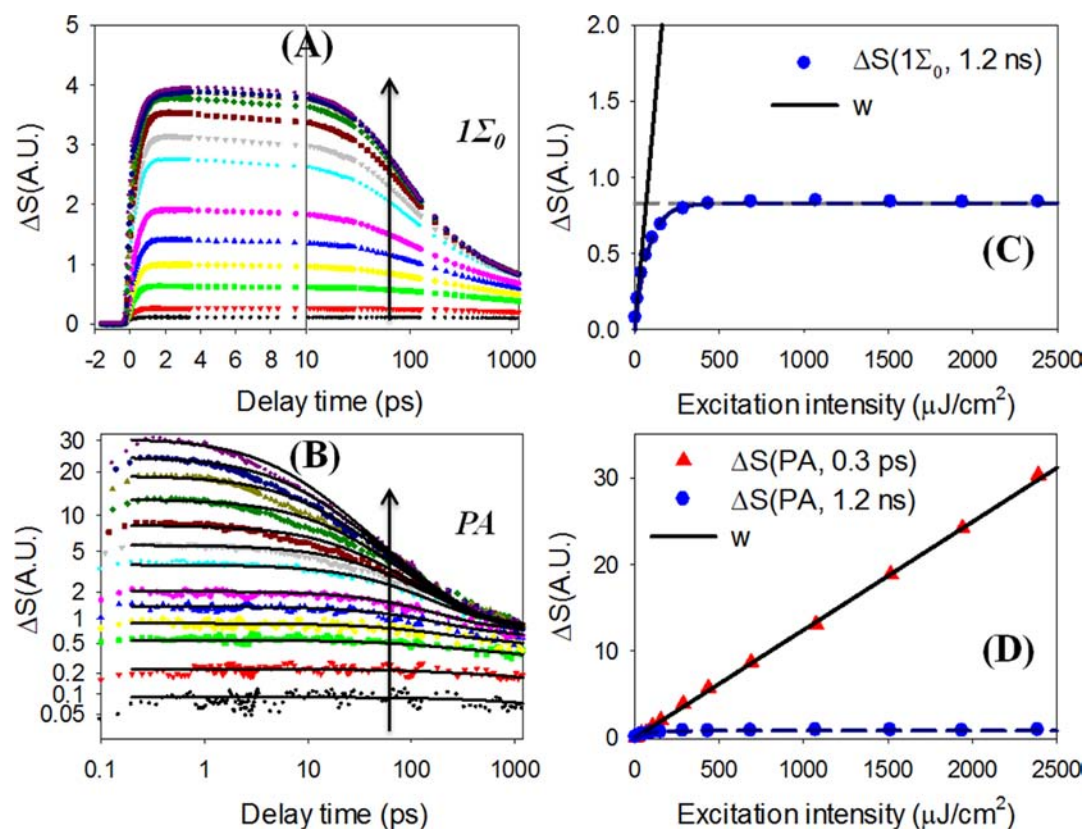


**Figure 3.** Left column: Normalized transient kinetics (symbols) at  $1\Sigma_0$  (A) and PA (B) under different excitation intensities. The solid lines in (B) are fits to a stochastic multicarrier annihilation model described in the main text. Right column: Normalized TA signal of  $1\Sigma_0$  (C) and PA (D) at indicated delay times as a function of excitation intensities. The solid and dashed lines are fits according to eqs 1–3.

excitation intensity dependence is consistent with the presence of a manifold of 1D exciton states.<sup>26,27</sup> With increasing number of excitons in the QR, 1D exciton states of higher energies are occupied, blue-shifting and broadening the bleach spectra. When all 1D exciton states in the  $1\Sigma$  band are occupied, the  $1\Sigma$  bleach spectrum resembles the steady-state absorption spectrum, which is the sum of all optically active transitions. At later delay time  $t_L$  (1.2 ns), the  $1\Sigma$  bleach peak positions under all excitation intensities merge to the same energy as the  $1\Sigma_0$  exciton, indicating the completion of the exciton–exciton annihilation in the QR and the formation of the long-lived  $1\Sigma_0$  single exciton state.

It should be noted that the observed excitation intensity dependent transient spectral evolution of the  $1\Sigma$  bleach in CdSe QRs is similar to the band filling induced dynamic Burstein–Moss shift observed in semiconductor materials with bulk-like continuous density of states.<sup>19,42,50</sup> It is different from the excitation intensity dependence of the two-fold degenerate 1S exciton bleach in CdSe QDs.<sup>17,19</sup> As a comparison, the excitation intensity dependent spectral evolution and steady-state absorption spectrum of CdSe QDs with similar lowest exciton energy (1S peak at 574 nm) are shown in SI10, Supporting Information. With increased number of excitons per QD, the initial amplitudes of the 1S bleach (at 1.5 ps) increase until it reaches saturation. More importantly, the 1S bleach peak shows negligible excitation intensity dependent peak shifting and broadening, and the bleach spectrum closely resembles the steady-state absorption spectrum at all excitation intensities. The power dependence of 1S exciton bleach amplitude can be well modeled by assuming a two-fold

degenerate exciton state (SI10, Supporting Information) with an initial Poisson distribution of the number of excitons in QDs, as previously reported.<sup>17,19</sup>

To quantify the exciton distribution and multiexciton Auger annihilation dynamics, we analyze the excitation intensity dependent  $1\Sigma_0$  and PA kinetics shown in Figure 3A,B. Let  $P(n,t)$  be the probability of having QRs with  $n$  excitons at delay time  $t$ . Because 400 nm excitation creates electron and hole pairs well above the band edge, the number of excitons ( $n$ ) per QR at early time ( $t_E = 0.3$  ps, after thermal relaxation and before annihilation) can be assumed to obey the Poisson distribution:

$$P(n, t_E) = f(n) = w^n e^{-w} / n! \quad (1)$$

where  $f(n)$  is the probability of having CdSe QRs with  $n$  excitons and  $w$  is the average number of excitons per QR. The latter is proportional to the excitation intensity ( $I$ ),  $w = C * I$ . The scaling factor  $C$  depends on the CdSe QR absorption cross section at the excitation wavelength and pump/probe beam geometries and overlap. Accurate determination of  $C$  is difficult experimentally.<sup>17,19,41</sup> Instead, we determine the average number of excitons by fitting the excitation intensity dependence of the signal amplitude (see below), which has been successfully applied to CdSe and CdSe/CdS QDs.<sup>17,19,41</sup>

With increasing excitation intensities, both  $1\Sigma_0$  and PA kinetics show larger amplitudes of fast decay components, consistent with the creation and annihilation of multiple excitons in the QR. After 1.2 ns ( $t_L$ ), the  $1\Sigma_0$  kinetics under all excitation intensities agree well with single exciton decay kinetics (SI3 and SI4, Supporting Information), indicating that

the signal at  $t_L = 1.2$  ns is solely due to the single exciton state. Therefore, at that time, the transient signal amplitudes  $\Delta A(\lambda, t_L)$  ( $\lambda = 1\Sigma_0$  and PA) are proportional to the number of excited QRs:  $\Delta A(\lambda, t_L) = \alpha(\lambda)\gamma[1 - f(0)]$ , where  $\alpha(\lambda)$  is a scaling factor proportional to the extinction coefficients at that wavelength and  $\gamma = 0.83$  accounts for the decay of single exciton states in 1.2 ns. We define a normalized transient signal  $\Delta S(\lambda, t_L)$  that represents the probability of finding excited QRs at  $t_L$  in the ensemble:

$$\Delta S(\lambda, t_L) = \Delta A(\lambda, t_L)/\alpha(\lambda) = \gamma[1 - f(0)] \quad (2)$$

$\Delta S(\lambda, t_L)$  should approach  $\gamma (= 0.83)$  when all QRs are excited, from which we can determine the scaling factor  $\alpha(\lambda)$  for  $1\Sigma_0$  and PA signals, respectively. The transient signal at other delay times,  $\Delta A(\lambda, t)$ , is then normalized by the same scaling factor, and the normalized kinetics  $\Delta S(\lambda, t) = \Delta A(\lambda, t)/\alpha(\lambda)$  are shown in Figure 3A,B.

Because of the intensity dependent width broadening and peak shifting of the  $1\Sigma$  band, the initial bleach amplitude does not scale linearly with the number of excitons. A quantitative analysis of this signal would require a detailed model of the structure and transition strength of the 1D exciton states within the  $1\Sigma$  manifold, which has not been attempted here. However, similar to CdSe<sup>16</sup> and CdSe/CdS core/shell QDs,<sup>19</sup> the PA signal in the CdSe QRs increases linearly with the excitation intensity (or the average number of excitons). Therefore, the normalized transient PA signal at early time can be defined as

$$\Delta S(\text{PA}, t_E) = \sum_n n f(n) = w \quad (3)$$

The normalized transient signals  $\Delta S(1\Sigma_0, t_L)$ ,  $\Delta S(\text{PA}, t_L)$ , and  $\Delta S(\text{PA}, t_E)$  are plotted as a function of excitation intensities in Figure 3C,D. These transient signals can be simultaneously fitted by eqs 1–3 with the scaling factor  $C$  as the only fitting parameter. This model describes well the experimental data, from which the scaling factor  $C$  and, thus, the average number of excitons at any excitation intensity can be obtained. As can be seen in Figure 3D, the normalized PA signal at early time follows the average number of excitons,  $w$ . At the highest excitation intensity ( $2390 \mu\text{J}\cdot\text{cm}^{-2}$ ), as many as 30 excitons in each CdSe QR are generated by multiphoton absorption and accommodated by the densely spaced 1D exciton states.

Since the PA signal is proportional to the average number of excitons per QR under all excitation intensities, the kinetics of the normalized PA signal  $\Delta S(\text{PA}, t)$  directly reflects the multiple exciton Auger annihilation process. At delay time  $t$ ,

$$\Delta S(\text{PA}, t) = \sum_n n P(n, t) \quad (4)$$

Assuming sequential multiexciton annihilation process ( $n \rightarrow n - 1, \dots, \rightarrow 2 \rightarrow 1$ ) in QRs and denoting the rate constant for the transition from  $n$  to  $n - 1$  exciton states by  $1/\tau_n$ , the time-dependent probability  $P(n, t)$  can be described by a set of coupled rate equations:<sup>13–16,51</sup>

$$\frac{dP(n, t)}{dt} = \frac{P(n+1, t)}{\tau_{n+1}} - \frac{P(n, t)}{\tau_n} \quad (5)$$

The Auger decay rate of an  $n$ -exciton state  $1/\tau_n$  ( $n > 1$ ) is expected to be (i)  $1/\tau_n = C_2/2(n(n-1))$  according to the excitonic model, in which the electrons and holes are bound as excitons and the Auger recombination occurs through exciton–exciton bimolecular collision or (ii)  $1/\tau_n = C_3/2(n^2(n-1))$

according to the independent carrier model, in which the electrons and holes are independent carriers and the Auger recombination involves three-carrier collisions.<sup>14–16,51</sup>

The normalized PA decay kinetics (Figure 3B) are fitted with eqs 4 and 5 according to the two Auger rate scaling models. The fit requires the single exciton ( $\tau_1$ ) and biexciton ( $\tau_2$ ) lifetimes and the initial distribution of excitons. The initial distribution  $P(n, t_E)$  of exciton states can be calculated using eq 1 for any given excitation intensities. The calculated distributions of the first three excitation intensities are listed in Table S6, Supporting Information. Under the lowest excitation intensity ( $7 \mu\text{J}\cdot\text{cm}^{-2}$ ), the excited QRs ( $n \geq 1$ ) are mostly in the single exciton state (97%) and show long-lived single exciton decay kinetics. Although the single exciton decay is a nonsingle exponential (Figure 1D), the  $1\Sigma_0$  bleach recovery kinetics within the first 1.2 ns, the relevant time window for the kinetics shown in Figure 3B, can be well represented by a single exponential decay with  $\tau_1 = 7$  ns. When the excitation intensity increases from 7 to  $17.6 \mu\text{J}\cdot\text{cm}^{-2}$ , the excited QR is still dominated by single exciton states (90.5%) with a small amount of biexciton state population (9.0%). The  $1\Sigma_0$  shows a fast decay component corresponding to the biexciton Auger annihilation (see Figure S14A, Supporting Information). Subtraction of the normalized (at 1.2 ns)  $1\Sigma_0$  kinetics under these two lowest excitation intensities yields the biexciton decay kinetics, from which we obtain the biexciton lifetime  $\tau_2$  of 201 ps. This biexciton lifetime is close to the values reported previously in similar CdSe QRs.<sup>49,52</sup> It is about four times longer than that of 0D biexcitons in CdSe QDs ( $\sim 50$  ps) with similar confinement energies,<sup>13,17</sup> which can be attributed to the much bigger volume along the axial direction in CdSe QRs.

The numerically simulated kinetics according to the excitonic model is shown in Figure 3B (black lines), and the fits according to the independent carrier behavior are plotted in Figure S7A, Supporting Information. It is clear that the excitonic model yields a much better fit to the experimental results than the independent carrier model, indicating that the Auger recombination in 1D QRs is dominated by exciton–exciton bimolecular annihilation. It is consistent with the formation of strongly bound 1D excitons in CdSe QRs. The agreement is remarkable considering that there are no fitting parameters in the simulation. At high average exciton numbers, the simulated decay kinetics is slower than the experimental result. The reason for the deviation is not clear. It may suggest a weakened Coulomb attraction for very high-order exciton states and/or spatially separated e–h pairs in some portions of CdSe QR because of wurtzite/zinc blend phase disorder.<sup>36,53</sup> As shown in Figure S7B, Supporting Information, a fit that includes a mixture of QR populations following excitonic (93%) and independent carrier (7%) Auger recombination models leads to a better agreement with the experimental results. The lifetimes of  $n$ -exciton states in CdSe QR calculated from the excitonic model are plotted in Figure 6B. Because of the reduced Auger rate constant due to their larger volume and the weaker dependence on  $n$ , QRs show a much longer-lived multiexciton states ( $\sim 2$  orders of magnitude) than typical QDs, and the difference becomes larger for higher order exciton states.

Earlier studies on Auger decay rates in CdSe QDs (and QRs) were based on the 1S ( $1\Sigma$ ) exciton bleach recovery kinetics and a bulk semiconductor kinetic model which neglects the distribution of exciton numbers in an ensemble.<sup>13,35</sup> An elaborated subtraction scheme was used to extract the second-

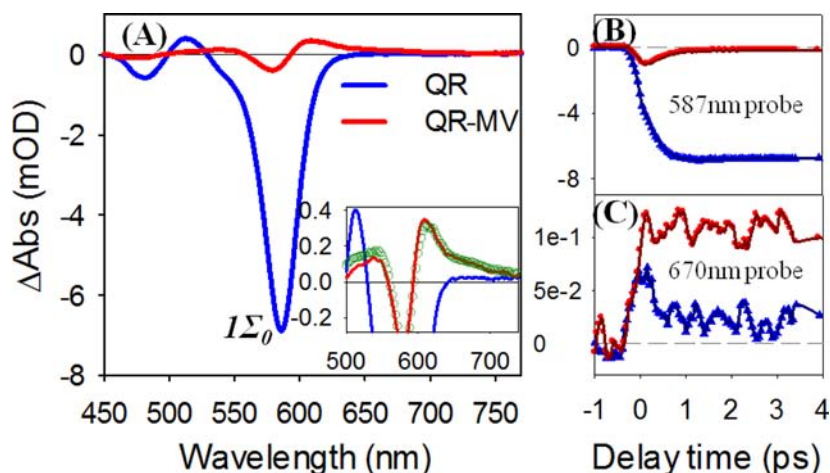


**Figure 4.** (A) TA spectrum of free CdSe QRs (blue) and CdSe QR–MV<sup>2+</sup> complexes (red) at 1.5 ps after 400 nm excitation (intensity: 7  $\mu\text{J}\cdot\text{cm}^{-2}$ ). Inset: An expanded view of the spectrum at 500–750 nm and a simulated spectrum of the charge-separated state (green circles) of the QR–MV<sup>2+</sup> complex. Comparison of TA kinetics probed at (B) 587 nm ( $1\Sigma_0$ ) and (C) 670 nm (MV<sup>+•</sup> radicals) in free CdSe QRs (blue triangles) and CdSe–MV<sup>2+</sup> complexes (red circles).

and third-order exciton state lifetimes and the ratio between them provides an initial sense of the multiexciton state lifetime scaling law. Because of the saturation of the two-fold degenerate  $1S$  bleach in QDs and shifting and broadening of densely spaced  $1\Sigma$  bleach in QRs as well as the quantized nature of the exciton number in a given NC, the validity of such approach for obtaining the lifetimes of higher order ( $\geq 3$ ) exciton states has been questioned.<sup>14,15</sup> Furthermore, our simulation result suggests that both the excitonic (Figure 3B) and independent carrier (Figure S7A, Supporting Information) models describe the kinetics reasonably well when the population of high order exciton states and average number of excitons per QD are small. Therefore, a rigorous test of the validity of these models requires the decay kinetics of higher order exciton states, as shown in Figure 3B and S7A, Supporting Information. Unlike the  $1S$  or  $1\Sigma$  interband transitions, the broad PA signal, whose amplitude depends linearly on the exciton number, offers a simple way to monitor the decay kinetics of higher order excitons. A similar approach has been recently applied to the multiexciton decay kinetics of 0D excitons in QDs, which was found to be well described by the  $n^2(n-1)$  Auger rate scaling law.<sup>16,19</sup>

**Single and Multiple Exciton Dissociation from CdSe QRs.** To examine the effect of 1D exciton structure on single and multiple exciton dissociation dynamics in CdSe QRs, we chose MV<sup>2+</sup>, a widely used electron mediator for photocatalytic reactions, as a model electron acceptor. The TA spectra of CdSe QRs with and without MV<sup>2+</sup> are compared in Figure 4A (at 1.5 ps) and S12, Supporting Information, (0–1.2 ns). These spectra were taken at the lowest excitation intensity (7  $\mu\text{J}\cdot\text{cm}^{-2}$ ) to ensure that the signal is dominated by single exciton states. Comparison of transient kinetics in free QRs and QR–MV<sup>2+</sup> complexes at 587 nm ( $1\Sigma_0$ ) and 670 nm (MV<sup>+•</sup> radical) is shown in Figure 4B,C, respectively. As discussed above,  $1\Sigma_0$  bleach of free CdSe QRs is long-lived, reflecting the long-lived single exciton state. In QR–MV<sup>2+</sup> complexes, the  $1\Sigma_0$  bleach grows to a much smaller initial amplitude and decays rapidly in the first 1 ps (Figure 4B), suggesting ultrafast (hot) ET from the CdSe QR to adsorbed MV<sup>2+</sup>. Concomitant with the  $1\Sigma_0$  bleach recovery, a spectrum with derivative-like feature below 650 nm and a positive absorption band above 650 nm is formed (Figure 4A inset). This spectrum can be

attributed to the charge-separated state of CdSe QR–MV<sup>2+</sup> complexes in which the electron is transferred to the adsorbed MV<sup>2+</sup> molecules and the hole remains in the CdSe QR. The buildup of the electric field shifts the excitonic transition in CdSe QRs through Stark effect, leading to the derivative-like features in the TA spectrum.<sup>54,55</sup> Such a charge separation induced Stark effect spectrum of QR can be clearly resolved in the QRs–benzoquinone (BQ) complex in which BQ/BQ<sup>-</sup> does not show any spectral signature in visible ranges (Figure S8, Supporting Information). In QR–MV<sup>2+</sup>, the stark effect spectrum extends until 650 nm, and beyond that the positive absorption band can be assigned to MV<sup>+•</sup> radicals and a small amount (15–20%) of QR PA signal. The spectrum of the charge-separated state in CdSe QR–MV<sup>2+</sup> complexes can be very well simulated by adding the TA spectrum of QR–BQ complexes (containing Stark effect and PA signal) and the MV<sup>+•</sup> radical signal (from CdS QD–MV<sup>2+</sup> complexes), confirming the spectral assignment (Figure S8, Supporting Information).

The MV<sup>+•</sup> radical kinetics can be monitored at 670 nm (Figure 4C), where the TA signal consists of MV<sup>+•</sup> radical absorption and a small amount of QR PA signal. As shown in Figure 4C, free CdSe QRs also show a positive absorption feature that decays within 1 ps and the long-lived PA absorption. The fast decay component corresponds to the red shift of the  $1\Sigma$  exciton band caused by hot carriers generated with 400 nm excitation (biexciton effect),<sup>41,56</sup> which can be clearly seen in Figure 1C. Indeed, with excitation near the band edge ( $\sim 590$  nm), the transient kinetics of free CdSe QRs at 670 nm does not show this hot carrier signature, and the corresponding kinetics of the CdSe–MV<sup>2+</sup> can be fit to yield a MV<sup>+•</sup> formation time, i.e., the electron-transfer (ET) time, of  $\sim 59$  fs, as shown in Figure S9, Supporting Information. This ET rate is much faster than the hot electron cooling process in the QR, which suggests that the majority of electrons go through ultrafast hot ET to MV<sup>2+</sup> prior to the relaxation to the  $1\sigma$  level.<sup>39</sup> This is consistent with the much smaller initial amplitude of the  $1\Sigma$  exciton bleach (Figure 4B). It is also interesting to point out that this ET rate is comparable to or even faster than that in CdSe QD–MV<sup>2+</sup> complexes.<sup>18,19,39,57</sup> Although the CdSe QR has a much bigger volume than typical QDs, it is still quantum confined in the radial direction. This

ensures a large amplitude of electron wave function at the surface, enabling ultrafast ET to the adsorbed electron acceptors.<sup>54</sup>

This fast ET rate, coupled with slow multiexciton Auger annihilation, suggests the possibility of efficient dissociation of multiple excitons from CdSe QRs. To determine the MED efficiency, TA measurements were conducted on the CdSe QR–MV<sup>2+</sup> complex under the same excitation intensities as in free CdSe QRs. The complete sets of TA spectra under different excitation intensities are shown in Figure S2, Supporting Information. Because of the negligible absorption of MV<sup>2+</sup> at the excitation wavelength (400 nm), the average numbers of excitons per QR created in the CdSe QR–MV<sup>2+</sup> complex should be the same as those in the free CdSe QR, which have been determined above. As shown in Figure 5A, the

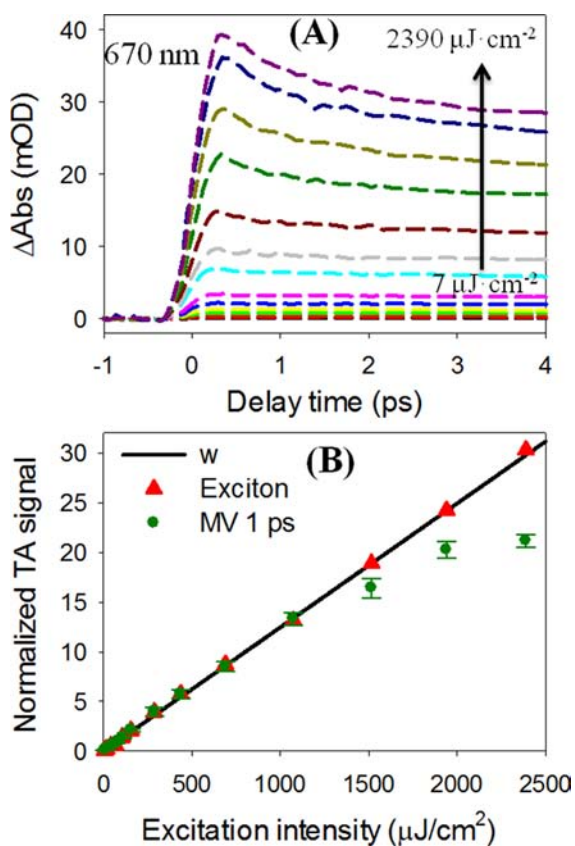


**Figure 5.** (A) Kinetics of MV<sup>+</sup>• radicals at 670 nm and (B) normalized MV<sup>+</sup>• radical signal at 1 ps as a function of excitation intensity in CdSe QR–MV<sup>2+</sup> complexes.

MV<sup>+</sup>• radical forms quickly and reaches a maximum at  $\sim 0.3$  ps under all excitation intensities. With increasing excitation intensities, the initial amplitude of 670 nm signal increases, and the decay due to bimolecular charge recombination process becomes faster, indicating more MV<sup>+</sup>• radicals are generated from each QR.<sup>17,19</sup>

In order to determine the average number of MV<sup>+</sup>• radicals generated per QR, we defined a normalized MV<sup>+</sup>• radical signal:  $S_{\text{MV}^+}(I, t) = \Delta A(\text{MV}^+, I, t) / \alpha(\text{MV}^+)$ , where  $\Delta A(\text{MV}^+, I, t)$  is the MV<sup>+</sup>• radical signal size at intensity  $I$  at delay time  $t$  and  $\alpha(\text{MV}^+)$  is a scaling factor.<sup>19</sup> As discussed above (and in SI6, Supporting Information), at the lowest three excitation intensities ( $I = 7.0, 17.6, 42.1 \mu\text{J}\cdot\text{cm}^{-2}$ ), the excited QR population is dominated by single exciton states with minor

biexciton states. Because the lifetimes of the single and biexciton states (see Figure 4B and S4B, Supporting Information) are much longer than the ET time, every exciton in the QR is assumed to be dissociated to generate one MV<sup>+</sup>• radical. This is consistent with the complete recovery of the  $1\Sigma$  exciton bleach in QR–MV<sup>2+</sup> complexes. Furthermore, because the MV<sup>+</sup>• radical kinetics under these low excitation intensities show negligible recombination loss in the first 5 ps, the normalized MV<sup>+</sup>• radical signal should be equal to the average number of dissociated excitons:  $S_{\text{MV}^+}(I, 1 \text{ ps}) = w$ . From the measured TA signal at the three lowest excitation intensities, a scaling factor  $\alpha(\text{MV}^+)$  was determined. The same scaling factor is applied to all MV<sup>+</sup>• radical signals  $\Delta A(\text{MV}^+, I, 1 \text{ ps})$  under different excitation intensities. We have chosen transient signal at 1 ps to avoid any contamination from the hot carrier induced exciton absorption signal. Furthermore, it has to be noted that the TA signal at 670 nm contains a small amount (15–20%) of PA signal from the holes in the QRs. The PA signal amplitude should be the same as that in free QRs and has been subtracted to yield the MV<sup>+</sup>• radical absorption signal shown in Figure 5B.

The normalized MV<sup>+</sup>• radical signal  $S_{\text{MV}^+}(I, 1 \text{ ps})$  represents the average number of MV<sup>+</sup>• radicals (or dissociated excitons) per QR. As shown in Figure 5B, at low excitation intensities ( $< 1200 \mu\text{J}\cdot\text{cm}^{-2}$ ) where charge recombination and Auger annihilation loss is negligible in the first 1 ps, the normalized MV<sup>+</sup>• radical signal closely follows the average number of excitons per QR ( $w$ ). At higher intensities, the normalized MV<sup>+</sup>• radical signal becomes smaller than  $w$ , because of charge recombination and the Auger annihilation loss. At highest excitation intensity ( $2390 \mu\text{J}\cdot\text{cm}^{-2}$ ), the number of excitons per QR that can be dissociated is  $21.2 \pm 0.6$ . The error bar reflects the standard deviation of two measurements.

It is interesting to compare the multiple exciton dissociation efficiency in CdSe QRs with CdSe QDs and CdSe/CdS core/shell QDs.<sup>20,25,26</sup> Using MV<sup>2+</sup> as electron acceptors, the multiexciton dissociation efficiency in CdSe QRs reported here is much higher than that in CdSe QDs ( $\sim 4$  excitons).<sup>18</sup> The efficiency of multiexciton dissociation depends on the competition between interfacial charge separation and multiexciton Auger annihilation. As shown in Figure 4, the quantum confinement in the radial direction in the QR facilitates ultrafast ET to MV<sup>2+</sup>, with a rate comparable to or even faster than that in QD–MV<sup>2+</sup> complexes.<sup>18,19,39,57</sup> Compared to QDs, the elongation along the axial direction increases the volume of the QR, which greatly reduces the Auger rate constant. Furthermore, the formation of strongly bound 1D exciton modifies the multiexciton Auger annihilation rate scaling law (Figure 6A), which further lengthens the  $n$ -exciton state lifetime in QRs compared to QDs, as shown in Figure 6B. Thus the reduced Auger recombination rate is responsible for the enhanced MED efficiency in CdSe QRs compared to CdSe QDs. Although Auger recombination rate can also be decreased in type II CdSe/CdS core/shell QDs by reducing the electron/hole overlap, compared to QRs, the  $n$ -exciton state lifetime decreases much more rapidly with  $n$  in core/shell QDs due to different scaling law, reducing the efficiency of multiple exciton dissociation.<sup>19</sup>

## CONCLUSION

In summary, by TA spectroscopy, we show the formation of bound 1D exciton states in CdSe QRs. Furthermore, the lifetime of  $n$ -exciton states is controlled by Auger recombination, which occurs primarily through an exciton–exciton

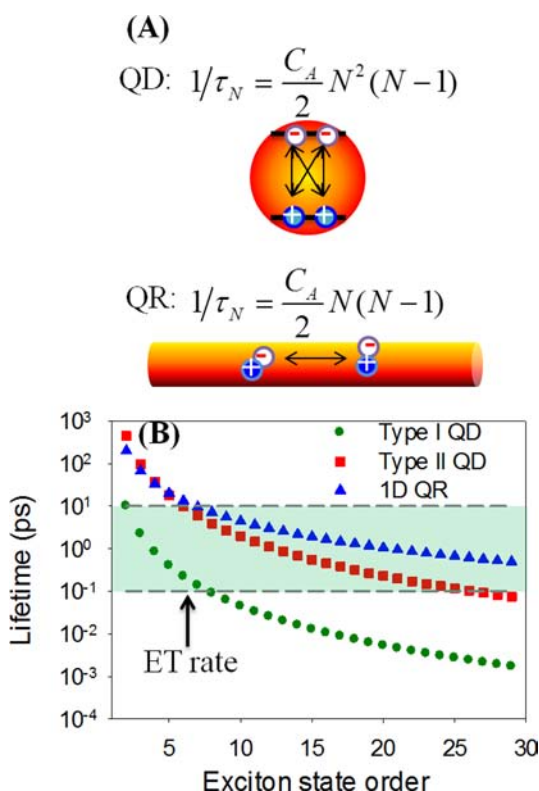


**Figure 6.** (A) Schematic depiction of multiexciton Auger annihilation process and the Auger rate scaling law in QDs (upper) and QRs (lower). (B) The lifetime of  $n$ -exciton states ( $n = 1-30$ ) of CdSe QDs (green circles),<sup>18</sup> quasi-type II CdSe/CdS QDs (red squares),<sup>19</sup> and CdSe QRs (blue triangles). Typical ET times from QDs and QRs to molecular adsorbates (100 fs to 10 ps) are indicated in the shaded area, suggesting that more efficient multiple exciton dissociation can be achieved in CdSe QRs and CdSe/CdS core/shell QDs than in CdSe QDs.

bimolecular collision process with rates proportional to  $n(n-1)$ , in contrast to the  $n^2(n-1)$  dependence in CdSe QDs. This weaker dependence on  $n$  and the larger volume in CdSe QRs greatly lengthen their multiexciton lifetimes compared to CdSe QDs of a similar optical gap. In the presence of electron acceptors, such as  $MV^{2+}$ , excitons can be dissociated by ultrafast interfacial ET. Because of quantum confinement along the radial direction of the rod, the ET rate from QRs is comparable to that in CdSe QDs. The combination of ultrafast ET and reduced Auger recombination rates significantly enhances multiexciton dissociation efficiency in CdSe QRs. Under high excitation intensity, more than 21 electrons can be transferred from one CdSe QR to adsorbed  $MV^{2+}$  molecules, greatly exceeding the MED efficiency of CdSe QDs. Our findings, together with large absorption cross section, improved charge transport, and enhanced multiexciton generation reported in these materials,<sup>25,31,53,58</sup> suggest that quantum confined 1D nanomaterials (NR and NW) are promising light harvesting and multielectron transferring materials for photocatalytic and optoelectronic devices.

## ■ ASSOCIATED CONTENT

### 📄 Supporting Information

Additional figures and tables showing experimental methods, TA spectra of QR and QR- $MV^{2+}$  at all excitation intensities from fs to  $\mu$ s,  $1\Sigma_0$  and PA signal assignment, simulation of PA

decay kinetics, and excitation intensity results of CdSe QDs of similar confinement energy. This material is available free of charge via the Internet at <http://pubs.acs.org>.

## ■ AUTHOR INFORMATION

### Corresponding Author

tlian@emory.edu

### Notes

The authors declare no competing financial interest.

## ■ ACKNOWLEDGMENTS

The authors gratefully acknowledge the support from the National Science Foundation (CHE-0848556).

## ■ REFERENCES

- (1) Coe, S.; Woo, W.-K.; Bawendi, M.; Bulovic, V. *Nature* **2002**, *420*, 800.
- (2) Colvin, V. L.; Schlamp, M. C.; Alivisatos, A. P. *Nature* **1994**, *370*, 354.
- (3) Klimov, V. I.; Ivanov, S. A.; Nanda, J.; Achermann, M.; Bezel, L.; McGuire, J. A.; Piryatinski, A. *Nature* **2007**, *447*, 441.
- (4) Kambhampati, P. *Acc. Chem. Res.* **2010**, *44*, 1.
- (5) Fisher, B.; Caruge, J. M.; Zehnder, D.; Bawendi, M. *Phys. Rev. Lett.* **2005**, *94*, 087403.
- (6) Osovsky, R.; Cheskis, D.; Kloper, V.; Sashchiuk, A.; Kroner, M.; Lifshitz, E. *Phys. Rev. Lett.* **2009**, *102*, 197401.
- (7) Sukhovatkin, V.; Hinds, S.; Brzozowski, L.; Sargent, E. H. *Science* **2009**, *324*, 1542.
- (8) Sambur, J. B.; Novet, T.; Parkinson, B. A. *Science* **2010**, *330*, 63.
- (9) Semonin, O. E.; Luther, J. M.; Choi, S.; Chen, H.-Y.; Gao, J.; Nozik, A. J.; Beard, M. C. *Science* **2011**, *334*, 1530.
- (10) Debnath, R.; Bakr, O.; Sargent, E. H. *Energy Environ. Sci.* **2011**, *4*, 4870.
- (11) Chan, W.-L.; Ligges, M.; Jailaubekov, A.; Kaake, L.; Miaja-Avila, L.; Zhu, X.-Y. *Science* **2011**, *334*, 1541.
- (12) Nair, G.; Chang, L.-Y.; Geyer, S. M.; Bawendi, M. G. *Nano Lett.* **2011**, *11*, 2145.
- (13) Klimov, V. I.; Mikhailovsky, A. A.; McBranch, D. W.; Leatherdale, C. A.; Bawendi, M. G. *Science* **2000**, *287*, 1011.
- (14) Klimov, V. I.; McGuire, J. A.; Schaller, R. D.; Rupasov, V. I. *Phys. Rev. B* **2008**, *77*, 195324.
- (15) Barzykin, A. V.; Tachiya, M. *J. Phys.: Condens. Matter* **2007**, *19*, 065105.
- (16) Ueda, A.; Tayagaki, T.; Kanemitsu, Y. *J. Phys. Soc. Jpn.* **2009**, *78*, 083706.
- (17) Huang, J.; Huang, Z.; Yang, Y.; Zhu, H.; Lian, T. *J. Am. Chem. Soc.* **2010**, *132*, 4858.
- (18) Matylytsky, V. V.; Dworak, L.; Breus, V. V.; Basche, T.; Wachtveitl, J. *J. Am. Chem. Soc.* **2009**, *131*, 2424.
- (19) Zhu, H.; Song, N.; Rodríguez-Córdoba, W.; Lian, T. *J. Am. Chem. Soc.* **2012**, *134*, 4250.
- (20) Hu, J.; Li, L.-s.; Yang, W.; Manna, L.; Wang, L.-w.; Alivisatos, A. P. *Science* **2001**, *292*, 2060.
- (21) Kan, S.; Mokari, T.; Rothenberg, E.; Banin, U. *Nat. Mater.* **2003**, *2*, 155.
- (22) Yu, H.; Li, J.; Loomis, R. A.; Gibbons, P. C.; Wang; Buhro, W. E. *J. Am. Chem. Soc.* **2003**, *125*, 16168.
- (23) Amirav, L.; Alivisatos, A. P. *J. Phys. Chem. Lett.* **2010**, *1*, 1051.
- (24) Tang, M. L.; Grauer, D. C.; Lassalle-Kaiser, B.; Yachandra, V. K.; Amirav, L.; Long, J. R.; Yano, J.; Alivisatos, A. P. *Angew. Chem., Int. Ed.* **2011**, *50*, 10203.
- (25) Tang, J.; Huo, Z.; Brittman, S.; Gao, H.; Yang, P. *Nat. Nano* **2011**, *6*, 568.
- (26) Shabaev, A.; Efros, A. L. *Nano Lett.* **2004**, *4*, 1821.
- (27) Bartnik, A. C.; Efros, A. L.; Koh, W. K.; Murray, C. B.; Wise, F. W. *Phys. Rev. B* **2010**, *82*, 195313.

- (28) Slachmuylders, A. F.; Partoens, B.; Magnus, W.; Peeters, F. M. *Phys. Rev. B* **2006**, *74*, 235321.
- (29) Muljarov, E. A.; Zhukov, E. A.; Dneprovskii, V. S.; Masumoto, Y. *Phys. Rev. B* **2000**, *62*, 7420.
- (30) Vietmeyer, F.; McDonald, M. P.; Kuno, M. K. *J. Phys. Chem. C* **2012**, *116*, 12379.
- (31) Protasenko, V.; Bacinello, D.; Kuno, M. *J. Phys. Chem. B* **2006**, *110*, 25322.
- (32) Chen, X.; Nazzal, A.; Goorskey, D.; Xiao, M.; Peng, Z. A.; Peng, X. *Phys. Rev. B* **2001**, *64*, 245304.
- (33) Carey, C. R.; LeBel, T.; Crisostomo, D.; Giblin, J.; Kuno, M.; Hartland, G. V. *J. Phys. Chem. C* **2010**, *114*, 16029.
- (34) Giblin, J.; Kuno, M. *J. Phys. Chem. Lett.* **2010**, *1*, 3340.
- (35) Htoon, H.; Hollingsworth, J. A.; Dickerson, R.; Klimov, V. I. *Phys. Rev. Lett.* **2003**, *91*, 227401.
- (36) Robel, I.; Bunker, B. A.; Kamat, P. V.; Kuno, M. *Nano Lett.* **2006**, *6*, 1344.
- (37) Vietmeyer, F.; Frantsuzov, P. A.; Janko, B.; Kuno, M. *Phys. Rev. B* **2011**, *83*, 115319.
- (38) Barzykin, A. V.; Tachiya, M. *Phys. Rev. B* **2005**, *72*, 075425.
- (39) Jiang, Z.-J.; Kelley, D. F. *J. Phys. Chem. C* **2011**, *115*, 4594.
- (40) Peng, Z. A.; Peng, X. *J. Am. Chem. Soc.* **2002**, *124*, 3343.
- (41) Klimov, V. I. *Annu. Rev. Phys. Chem.* **2007**, *58*, 635.
- (42) Puthussery, J.; Lan, A.; Kosel, T. H.; Kuno, M. *ACS Nano* **2008**, *2*, 357.
- (43) Mohamed, M. B.; Burda, C.; El-Sayed, M. A. *Nano Lett.* **2001**, *1*, 589.
- (44) Burda, C.; Link, S.; Mohamed, M.; El-Sayed, M. *J. Phys. Chem. B* **2001**, *105*, 12286.
- (45) McArthur, E. A.; Morris-Cohen, A. J.; Knowles, K. E.; Weiss, E. A. *J. Phys. Chem. B* **2010**, *114*, 14514.
- (46) Huang, J.; Huang, Z.; Jin, S.; Lian, T. *J. Phys. Chem. C* **2008**, *112*, 19734.
- (47) Song, N.; Zhu, H.; Jin, S.; Lian, T. *ACS Nano* **2011**, *5*, 8750.
- (48) Knowles, K. E.; McArthur, E. A.; Weiss, E. A. *ACS Nano* **2011**, *5*, 2026.
- (49) Taguchi, S.; Saruyama, M.; Teranishi, T.; Kanemitsu, Y. *Phys. Rev. B* **2011**, *83*, 155324.
- (50) Burstein, E. *Phys. Rev.* **1954**, *93*, 632.
- (51) Wang, F.; Dukovic, G.; Knoesel, E.; Brus, L. E.; Heinz, T. F. *Phys. Rev. B* **2004**, *70*, 241403.
- (52) Jiang, Z.-J.; Kelley, D. F. *J. Phys. Chem. C* **2010**, *114*, 17519.
- (53) Kuno, M. *Phys. Chem. Chem. Phys.* **2008**, *10*, 620.
- (54) Zhu, H.; Song, N.; Lian, T. *J. Am. Chem. Soc.* **2010**, *132*, 15038.
- (55) Zhu, H.; Song, N.; Lian, T. *J. Am. Chem. Soc.* **2011**, *133*, 8762.
- (56) Klimov, V. I. *J. Phys. Chem. B* **2000**, *104*, 6112.
- (57) Morris-Cohen, A. J.; Frederick, M. T.; Cass, L. C.; Weiss, E. A. *J. Am. Chem. Soc.* **2011**, *133*, 10146.
- (58) Cunningham, P. D.; Boercker, J. E.; Foos, E. E.; Lumb, M. P.; Smith, A. R.; Tischler, J. G.; Melinger, J. S. *Nano Lett.* **2011**, *11*, 3476.